

Mechanics Based Design of Structures and Machines

An International Journal

ISSN: (Print) (Online) Journal homepage: <https://www.tandfonline.com/loi/lmbd20>

A closed-form solution for asymmetric free vibration analysis of composite cylindrical shells with metamaterial honeycomb core layer based on shear deformation theory

Hamidreza Eipakchi & Farid Mahboubi Nasrekani

To cite this article: Hamidreza Eipakchi & Farid Mahboubi Nasrekani (2022): A closed-form solution for asymmetric free vibration analysis of composite cylindrical shells with metamaterial honeycomb core layer based on shear deformation theory, *Mechanics Based Design of Structures and Machines*, DOI: [10.1080/15397734.2022.2051183](https://doi.org/10.1080/15397734.2022.2051183)

To link to this article: <https://doi.org/10.1080/15397734.2022.2051183>



Published online: 17 Mar 2022.



Submit your article to this journal [↗](#)



View related articles [↗](#)



View Crossmark data [↗](#)



A closed-form solution for asymmetric free vibration analysis of composite cylindrical shells with metamaterial honeycomb core layer based on shear deformation theory

Hamidreza Eipakchi^a  and Farid Mahboubi Nasrekani^b 

^aFaculty of Mechanical and Mechatronics Engineering, Shahrood University of Technology, Shahrood, I.R. Iran;

^bSchool of Information Technology, Engineering, Mathematics and Physics, The University of the South Pacific (USP), Suva, Fiji

ABSTRACT

Asymmetric free vibration analysis of composite cylindrical shells with a honeycomb core layer and adjustable Poisson's ratio is performed analytically in this study. The equations of motion which are a system of coupled partial differential equations are extracted using Hamilton's principle by employing the first-order shear deformation theory and they are solved analytically. To study the sensitivity of the results to the different parameters of the honeycomb structure, geometrical parameters, and boundary conditions, a parametric study is presented. It is concluded that for the auxetic composite shell with a negative Poisson's ratio, by decreasing the Poisson ratio, the frequency decreases. Also, it is shown that by employing the composite shells the weight decreases significantly, while the asymmetric frequency will not change remarkably. By adjusting the Poisson ratio, the frequency variations are studied for a composite shell with a honeycomb core layer. The results are compared with the finite element method and some other references.

ARTICLE HISTORY

Received 1 July 2021

Accepted 2 March 2022


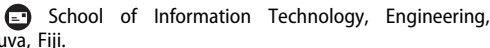
KEYWORDS

Asymmetric vibration;
composite cylindrical shell;
honeycomb core layer;
adjustable Poisson's ratio;
first-order shear
deformation theory;
closed-form solution

1. Introduction

Honeycomb structures are materials with minimal density and relatively high out-of-plane shear and compression characteristics. In order to provide strength in tension, the honeycomb structures are usually made by layering between two isotropic layers. Nowadays, due to the lightness, high specific strength, and high energy absorption, applications of the honeycomb structures are greatly increased. The free vibration analysis and determination of natural frequencies have been done in some research but only a few studies especially for honeycomb structures were conducted by considering the asymmetric conditions, while, in the real world most of the cases are categorized under asymmetric conditions.

Chen and Babcock (1975) analyzed large-amplitude asymmetric vibrations of isotropic thin cylindrical shells based on the Donnell shallow shell theory and using the perturbation technique. Raju and Rao (1976) presented a finite element (FE) method to analyze the large amplitude asymmetric vibrations of isotropic shells of revolution based on the Sander nonlinear theory. Sivadas and Ganesan (1991) studied the asymmetric vibration of isotropic and composite shells of revolution with variable thickness based on the Naghdi theory and employing the FE method.

CONTACT Farid Mahboubi Nasrekani  Nasrekani_f@usp.ac.fj 
Communicated by Eleonora Tubaldi.

Ganapathi and Varadan (1996) studied the nonlinear free vibrations of isotropic thin cylindrical shells using the FE method and by employing the Mindlin and von Karman theories. Akyuz and Ertepinar (1999) investigated the stability and asymmetric vibrations of isotropic, homogeneous, hyperelastic cylindrical shells under uniform radial tensile or compressive load using the shooting and FE methods. Singh, Yadav, and Iyengar (2002) obtained the effect of the variations of the mechanical properties of laminated composite cylindrical panels on its natural frequency using the higher-order shear deformation theory and FE method. By applying spline function approximations and point collocation method a free vibration analysis of circular thin layered shells has been studied by Viswanathan and Navaneethakrishnan (2003) based on Love's theory. Ozerciyes and Yuceoglu (2008) investigated free asymmetric vibrations of composite cylindrical shells based on the Timoshenko-Mindlin theory. The governing equations were solved numerically using the modified transfer matrix method with Chebyshev polynomials. Garg, Khare, and Kant (2006) presented a closed-form solution for the free vibrational behavior of simply supported laminated composite shells based on the higher-order shear deformation theory, Sander's theory, and using the Navier technique. Wahl et al. (2012) conducted an analytical, numerical, and experimental study on the shear stress in the honeycomb layer of composite plates using the FE method. Zhang, Hao, and Yang (2012) studied the nonlinear dynamic behavior of a functionally graded (FG) circular cylinder with clamped boundary conditions (BCs) subjected to an external loading based on the first-order shear deformation theory (FSDT) and von Karman relations and by employing the Galerkin method. Wang et al. (2013) determined an approximate solution of natural frequencies for anisotropic glass-fiber-reinforced plastic cylindrical shells with asymmetric BCs using Love's theory. Isvandzibaei, Jamaluddin, and Raja Hamzah (2014) studied the natural frequency of thin multiple layered cylindrical shells subjected to lateral pressure based on Love's theory and the Ritz method. The cylindrical shell consisted of two inner and outer steel layers and one aluminum core layer. Zhang et al. (2014) investigated the nonlinear behavior of a three-dimensional Kagome truss core sandwich plate with simply supported BCs using the third-order shear deformation theory and von Karman relations. The governing equations were solved using the Galerkin method. Liu et al. (2015) conducted a nonlinear vibrational analysis of an FG cylindrical shell with simply supported BCs and initial geometric imperfection subjected to complex load. The equations were obtained using third-order shear deformation theory and von Karman relations and they were solved by applying the Galerkin method. Khan, Patel, and Nath (2015) presented a free and forced vibration analysis for bimodular cross-ply laminated cylindrical shells using Bert's model and the FSDT employing a numerical procedure by the iterative method. Javed, Viswanathan, and Aziz (2016) proposed a numerical solution for free vibration analysis of composite cylindrical shells with variable thickness by employing spline approximation and the FSDT. Thin and Nguyen (2016) proposed a new model for free vibration analysis of composite cylindrical shells filled with fluid based on the dynamic stiffness method or continuous elements using the Reissner-Mindlin theory. Mohammadimehr and Mehrabi (2017) investigated the free vibration and stability of double-bonded micro composite sandwich cylindrical shells conveying fluid flow under magneto-thermo-mechanical loadings based on Reddy cylindrical double-shell theory and using modified couple stress theory and generalized differential quadrature method. Liu, Zhang, and Wang (2017) studied the nonlinear vibrations of a composite laminated cylindrical shell with clamped BCs and radial pre-stretched membranes at both ends using the third-order shear deformation theory and nonlinear von Karman relations. The solution was extracted by employing the Galerkin method. Biswal and Mohanty (2018) proposed a shear deformable shell element to study the free vibration of doubly curved sandwich panels with viscoelastic core based on the FE method. Zhu et al. (2019) investigated the natural frequency and energies of honeycomb sandwich plate using the third-order shear deformation theory, von Karman nonlinear relations, and Hamilton energy method. Bagheri, Kiani, and Eslami (2018) studied the free vibration of isotropic joined conical-cylindrical-conical shells based on the FSDT and the

equations were solved using the generalized differential quadrature method. Zhang, Liu, et al. (2018) investigated the nonlinear vibrations of a carbon fiber reinforced polymer laminated cylinder using the FSDT and von Karman relations. The solution was based on the Galerkin method. Wang et al. (2018) analyzed free vibrations and static bending of FG graphene nanoplatelet reinforced composite shells with simply supported BCs. The equations were derived using the higher-order shear deformation theory and the solution was based on the Navier technique. Zhang, Liu, et al. (2018) studied the resonant responses of a composite laminated cylindrical shell clamped along a generatrix and radially pre-stretched membranes at both ends using the multiple-scale method. Liu et al. (2019) investigated the nonlinear vibrations of an eccentric rotating composite laminated cylinder based on the Donnell thin shear deformation theory and von Karman relations. The equations were solved by applying the Galerkin method. Li, Pang, et al. (2019) presented a solution for the free vibration of non-Levy-type cylindrical shell panels using a Hamiltonian system-based superposition method. Nekouei, Raghebi, and Mohammadi (2019) investigated the vibrational behavior of composite conical shells reinforced with shape memory alloy fibers, based on the classical shell theory and von Karman theory. The governing equations were solved by employing the generalized differential quadrature method. Li, Pang, et al. (2019) presented a semi-analytical method to study the free vibration behavior of laminated cylindrical and spherical shells based on the multi-segment partitioning, the FSDT, and Rayleigh-Ritz method. Lopatin and Morozov (2019) studied the free vibrational behavior of a composite cylindrical shell with a rigid weightless disk that is attached to its end. By employing the Ritz method, the axisymmetric frequencies were obtained. Li, Yao, and Wang (2020) investigated the flexural vibration of honeycomb sandwich cylindrical shell experimentally and FE method. The free and forced vibration problem of an axisymmetric auxetic composite shell was solved by Eipakchi and Mahboubi Nasrekani (2020) using the classical plate theory (CPT) and Galerkin's method under moving internal pressure. Eipakchi, Mahboubi Nasrekani, and Ahmadi (2020) presented an analytical method to investigate the free and forced vibrational behavior of axisymmetric viscoelastic shells under moving load using the CPT. Eipakchi and Mahboubi Nasrekani (2020) studied the nonlinear vibrational behavior of viscoelastic axisymmetric cylindrical shells using CPT, von Karman theory, and by employing the method of multiple scale. Eipakchi and Mahboubi Nasrekani (2020) solved the equilibrium equations of auxetic composite cylindrical shells with variable thickness and axisymmetric conditions using matched asymptotic expansion method and FSDT. The composite shell was made of three layers with a honeycomb core layer. Safarpour, Rahimi, and Alibeigloo (2020) carried out static and free vibration analysis of FG graphene platelets-reinforced composite conical shells, cylindrical shells, and annular plates based on the three-dimensional elasticity theory. The solution procedure was proposed using the differential quadrature method. Shahgholian-Ghahfarokhi et al. (2022) studied the free vibrational behavior of sandwich cylindrical shells with grid cores using experimental and FE methods. Banijamali and Jafari (2021) investigated the free vibration behavior of a rotating FG conical shell based on the CPT. The conical shell was reinforced by an anisogrid lattice structure. The governing equations were solved using the Galerkin method. Li, Zhou, and Zheng (2021) presented an analytical procedure for free vibration analysis of doubly curved shells using the symplectic superposition method. Bagheri et al. (2021) analyzed the free vibration of an FG cylindrical shell closed with two hemispherical caps based on the first-order theory of shells and Donnell equations and the equations of motion were solved using the generalized differential quadrature method. Wang et al. (2021) evaluated the response of corrugated core composite metal sandwich structures under fluid-structure interaction by employing a numerical model in ABAQUS. Eipakchi and Mahboubi Nasrekani (2021) presented an analytical method for nonlinear free vibration analysis of composite cylindrical shells with honeycomb core layer under axisymmetric conditions based on the FSDT and nonlinear von Karman relations and using the multiple-scale method.

There is a lot of research that studied the vibrational behavior of isotropic or traditional composite cylindrical shells under asymmetric conditions using a numerical method such as the FE method, which is a complicated and time-consuming procedure, especially for honeycomb structures. In this study, an analytical method is proposed to investigate the free vibrational behavior of asymmetric composite cylindrical shells with adjustable Poisson's ratio using the FSDT. There are some analytical studies in this field (e.g., Eipakchi and Mahboubi Nasrekani (2020) and Eipakchi and Mahboubi Nasrekani (2021)) that do not consider the asymmetric conditions and in this study, the effects of this condition on the free vibrational behavior of composite shells have been studied. It should be mentioned that frequencies have been affected by considering the asymmetric conditions and the governing equations have been changed. It is observed that axisymmetric frequency is not necessarily the minimum frequency and for some cases, the frequency of asymmetric case is less than the axisymmetric case. The different BCs are investigated and the effect of honeycomb structure on the natural frequency and mode shapes are studied and compared with the axisymmetric cases. The effect of different parameters of the honeycomb structure on the Poisson ratio has been studied by employing a parametric study and the effect of Poisson's ratio on the vibrational behavior of the composite shell is presented. The following key points are considered in this study:

- **Geometry:** The composite shell is an asymmetric finite-length cylindrical shell with three layers.
- **Material:** The inner and outer layers are made of isotropic materials and the core layer is a honeycomb structure with a negative Poisson's ratio. The thickness of the isotropic layers can be equal or unequal.
- **Theory:** The displacement field is considered according to the FSDT in asymmetric conditions. The stress-strain relations of the honeycomb core layer are obtained based on the plane stress theory and the isotropic layers have been extracted according to the three-dimensional theory of elasticity.
- **Solution method:** The solution procedure is proposed based on the mathematical methods to perform a parametric study on the free vibrational behavior of composite cylindrical shells with adjustable Poisson's ratio.

2. Equations of motion

An auxetic composite cylindrical shell with a honeycomb core layer of thickness h_2 and two inner and outer isotropic layers of thickness h_1 and h_3 respectively and length L has been considered as Fig. 1. R_m is the radius of the mid-plane and the origin of the coordinate system is assumed on this point. By employing the cylindrical coordinates the location of each point is defined by three parameters r , x , and θ , where $r=R_m+z$, and z is a variable measured from the mid-plane of the shell. The thickness of the isotropic layers (h_1 and h_3) can be either equal or unequal. Figure 1 shows the geometry of the honeycomb cell structure in which p , l , q , and φ are the thickness of the cell wall, length of the inclined cell rib, length of the vertical cell rib, and inclined angle, respectively.

The honeycomb properties are defined as the following (Li, Yao, and Wang 2020; Eipakchi and Mahboubi Nasrekani, 2020):

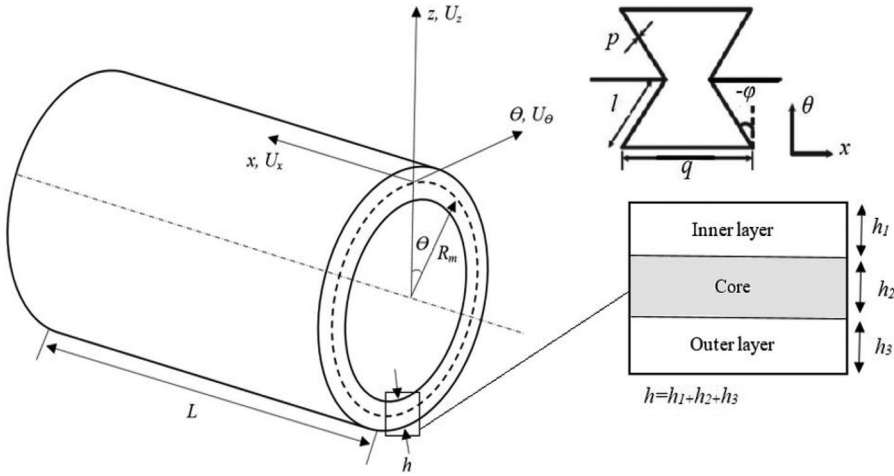


Figure 1. Geometry and schematic of composite cylindrical shell and honeycomb cell structure.

$$\begin{aligned}
 E_x^C &= \frac{E \cdot a_p^3}{\cos \phi (a_q + \sin \phi) (\tan^2 \phi + a_p^2)}; & E_\theta^C &= \frac{E \cdot a_p^3 (a_q + \sin \phi)}{\cos^3 \phi (1 + a_p^2 (\tan^2 \phi + a_q \sec^2 \phi))} \\
 \nu_{x\theta}^C &= \frac{\sin \phi (1 - a_p^2)}{(a_q + \sin \phi) (\tan^2 \phi + a_p^2)}; & \nu_{\theta x}^C &= \frac{\sin \phi (1 - a_p^2) (a_q + \sin \phi)}{\cos^2 \phi (1 + a_p^2 (\tan^2 \phi + a_q \sec^2 \phi))} \\
 G_{xz}^C &= \frac{G \cdot a_p \cos \phi}{a_q + \sin \phi}; & G_{x\theta}^C &= \frac{E a_p^3}{a_q (1 + 2a_q) \cos \phi}; & G_{z\theta}^C &= \frac{G a_p}{2 \cos \phi} \left(\frac{a_q + \sin \phi}{1 + 2a_q} + \frac{a_q + 2 \sin^2 \phi}{2(a_q + \sin \phi)} \right) \\
 \rho^C &= \rho \frac{a_p (a_q + 2)}{2 \cos \phi (a_q + \sin \phi)}; & a_p &= \frac{p}{l}; & a_q &= \frac{q}{l}
 \end{aligned} \tag{1}$$

where ρ , ν , E , and G are density, Poisson's ratio, Young's modulus, and shear modulus of the isotropic original material, respectively. The superscript c indicates the core layer properties. According to Eq. (1), it is observed that Poisson's ratio of the honeycomb structure is negative for the negatively inclined angle ϕ . By employing the FSDT for the asymmetric case, the displacement field is defined as the following:

$$U_x = u_0(x, \theta, t) + z u_1(x, \theta, t); \quad U_\theta = v_0(x, \theta, t) + z v_1(x, \theta, t); \quad U_z = w_0(x, \theta, t) \tag{2}$$

where U_x , U_θ , and U_z are displacement components in x , θ , and z directions, respectively. u_0 , v_0 , and w_0 are displacement components of the mid-plane, and u_1 , v_1 , and w_1 are unknown functions of x , θ , and t . The small-strain relations are as the following (Gibson and Ashby 1997):

$$\begin{aligned}
 \varepsilon_x &= \frac{\partial U_x}{\partial x} = \frac{\partial u_0}{\partial x} + z \frac{\partial u_1}{\partial x}; & \varepsilon_z &= \frac{\partial U_z}{\partial z} = 0; & \varepsilon_\theta &= \frac{U_z}{r} + \frac{1}{r} \frac{\partial U_\theta}{\partial \theta} = \frac{w_0}{r} + \frac{1}{r} \left(\frac{\partial v_0}{\partial \theta} + z \frac{\partial v_1}{\partial \theta} \right) \\
 \gamma_{z\theta} &= \frac{\partial U_\theta}{\partial z} + \frac{1}{r} \frac{\partial U_z}{\partial \theta} - \frac{U_\theta}{r} = v_1 + \frac{1}{r} \left(\frac{\partial w_0}{\partial \theta} \right) - \frac{v_0 + z v_1}{r}; & \gamma_{xz} &= \frac{\partial U_z}{\partial x} + \frac{\partial U_x}{\partial z} = \frac{\partial w_0}{\partial x} + u_1 \\
 \gamma_{x\theta} &= \frac{1}{r} \frac{\partial U_x}{\partial \theta} + \frac{\partial U_\theta}{\partial x} = \frac{1}{r} \left(\frac{\partial u_0}{\partial \theta} + z \frac{\partial u_1}{\partial \theta} \right) + \frac{\partial v_0}{\partial x} + z \frac{\partial v_1}{\partial x}
 \end{aligned} \tag{3}$$

The stress-strain relations for the composite shell are as the following (Eipakchi and Mahboubi Nasrekani, 2020; Sadd 2009):

$$\begin{aligned} \begin{Bmatrix} \sigma_x \\ \sigma_\theta \\ \sigma_z \end{Bmatrix}^{Outer} &= \begin{Bmatrix} \sigma_x \\ \sigma_\theta \\ \sigma_z \end{Bmatrix}^{Inner} = \begin{bmatrix} A & \lambda & \lambda \\ \lambda & A & \lambda \\ \lambda & \lambda & A \end{bmatrix} \begin{Bmatrix} \varepsilon_x \\ \varepsilon_\theta \\ \varepsilon_z \end{Bmatrix} \\ \tau_{xz}^{Outer} &= \tau_{xz}^{Inner} = \mu\gamma_{xz}; \quad \tau_{x\theta}^{Outer} = \tau_{x\theta}^{Inner} = \mu\gamma_{x\theta}; \quad \tau_{\theta z}^{Outer} = \tau_{\theta z}^{Inner} = \mu\gamma_{\theta z} \end{aligned} \quad (4a)$$

$$\begin{aligned} \begin{Bmatrix} \sigma_x \\ \sigma_\theta \end{Bmatrix}^{Core} &= \frac{1}{1 - \nu_{x\theta}^C \nu_{\theta x}^C} \begin{bmatrix} E_x^C & \nu_{x\theta}^C E_\theta^C \\ \nu_{x\theta}^C E_\theta^C & E_\theta^C \end{bmatrix} \begin{Bmatrix} \varepsilon_x \\ \varepsilon_\theta \end{Bmatrix}; \quad \sigma_z^{Core} = 0 \\ \tau_{xz}^{Core} &= G_{xz}^C \gamma_{xz}; \quad \tau_{x\theta}^{Core} = G_{x\theta}^C \gamma_{x\theta}; \quad \tau_{\theta z}^{Core} = G_{\theta z}^C \gamma_{\theta z} \end{aligned} \quad (4b)$$

where $A = \lambda + 2\mu$, λ , and μ are Lamé's constants. According to Eqs. (4), the stress-strain relations of the honeycomb core layer are defined based on the plane stress assumptions, and the stress-strain relations of the isotropic inner and outer layers are defined based on the generalized three-dimensional Hooke's law. The kinetic energy is defined as the following:

$$\begin{aligned} T &= \frac{R_m}{2} \int \int \sum_{i=1}^3 \int_{z_i}^{z_{i+1}} \rho_i \left(\left(\frac{\partial U_x}{\partial t} \right)^2 + \left(\frac{\partial U_z}{\partial t} \right)^2 + \left(\frac{\partial U_\theta}{\partial t} \right)^2 \right) \left(1 + \frac{z}{R_m} \right) dz dx d\theta \\ T &= R_m \int \int \left\{ C_1 \left[\left(\frac{\partial u_0}{\partial t} \right)^2 + \left(\frac{\partial v_0}{\partial t} \right)^2 + \left(\frac{\partial w_0}{\partial t} \right)^2 \right] + C_2 \left[\left(\frac{\partial u_1}{\partial t} \right)^2 + \left(\frac{\partial v_1}{\partial t} \right)^2 \right] \right. \\ &\quad \left. + C_3 \left(\frac{\partial u_0}{\partial t} \frac{\partial u_1}{\partial t} + \frac{\partial v_0}{\partial t} \frac{\partial v_1}{\partial t} \right) \right\} dx d\theta \\ z_1 &= -\left(h_3 + \frac{h_2}{2} \right); \quad z_2 = -\frac{h_2}{2}; \quad z_3 = \frac{h_2}{2}; \quad z_4 = \frac{h_2}{2} + h_1; \quad \rho_1 = \rho^{inner}; \quad \rho_2 = \rho^c; \quad \rho_3 = \rho^{outer} \end{aligned} \quad (5)$$

where C_1 , C_2 , and C_3 are constant coefficients, and they are reported in the [Appendix](#). The strain energy is defined as the following (Rao 2007):

$$\begin{aligned} U &= \frac{R_m}{2} \int \int \sum_{i=1}^3 \int_{z_i}^{z_{i+1}} \left(\sigma_x^i \varepsilon_x + \sigma_\theta^i \varepsilon_\theta + \sigma_z^i \varepsilon_z + \tau_{xz}^i \gamma_{xz} + \tau_{x\theta}^i \gamma_{x\theta} + \tau_{\theta z}^i \gamma_{\theta z} \right) \left(1 + \frac{z}{R_m} \right) dz dx d\theta \\ \sigma_j^1 &= \sigma_j^{inner}; \quad \sigma_j^2 = \sigma_j^c; \quad \sigma_j^3 = \sigma_j^{outer}; \quad j = x, z, \theta \\ \tau_k^1 &= \tau_k^{inner}; \quad \tau_k^2 = \tau_k^{core}; \quad \tau_k^3 = \tau_k^{outer}; \quad k = xz, \theta z, x\theta \end{aligned} \quad (6)$$

The stress resultants are defined as the following:

$$\begin{aligned} \{N_x M_x\} &= \sum_{i=1}^3 \int_{z_i}^{z_{i+1}} \{1, z\} \sigma_x^i \left(1 + \frac{z}{R_m} \right) dz; \quad \{N_\theta M_\theta\} = \sum_{i=1}^3 \int_{z_i}^{z_{i+1}} \{1, z\} \sigma_\theta^i dz; \quad Q_{xz} = \sum_{i=1}^3 \int_{z_i}^{z_{i+1}} \kappa \tau_{xz}^i \left(1 + \frac{z}{R_m} \right) dz \\ \{Q_{x\theta} M_{x\theta}\} &= \sum_{i=1}^3 \int_{z_i}^{z_{i+1}} \{1, z\} \tau_{x\theta}^i \left(1 + \frac{z}{R_m} \right) dz; \quad \{Q_{x\theta 0} M_{x\theta 0}\} = \sum_{i=1}^3 \int_{z_i}^{z_{i+1}} \{1, z\} \tau_{x\theta}^i dz; \quad Q_{\theta z} = \sum_{i=1}^3 \int_{z_i}^{z_{i+1}} \kappa \tau_{\theta z}^i \left(1 + \frac{z}{R_m} \right) dz; \\ \{Q_{\theta z 0} M_{\theta z 0}\} &= \sum_{i=1}^3 \int_{z_i}^{z_{i+1}} \kappa \{1, z\} \tau_{\theta z}^i dz; \end{aligned} \quad (7)$$

where κ is the shear correction factor and it is assumed $\kappa = 5/6$ [36]. By applying the Hamilton principle as $\delta \int_{t_1}^{t_2} (T - U) dt = 0$ (Rao 2007) and using Eqs. (5)–(7), the equations of motion are extracted as the following in terms of the stress resultants:

$$-2C_1 \frac{\partial^2 u_0}{\partial t^2} - C_3 \frac{\partial^2 u_1}{\partial t^2} + \frac{\partial N_x}{\partial x} + \frac{1}{R_m} \frac{\partial Q_{x\theta 0}}{\partial \theta} = 0 \quad (8a)$$

$$-2C_2 \frac{\partial^2 u_1}{\partial t^2} - C_3 \frac{\partial^2 u_0}{\partial t^2} + \frac{\partial M_x}{\partial x} - Q_{xz} + \frac{1}{R_m} \frac{\partial M_{x\theta}}{\partial \theta} = 0 \quad (8b)$$

$$-2C_1 \frac{\partial^2 v_0}{\partial t^2} - C_3 \frac{\partial^2 v_1}{\partial t^2} + \frac{Q_{\theta z}}{R_m} + \frac{1}{R_m} \frac{\partial N_\theta}{\partial \theta} + \frac{\partial Q_{x\theta}}{\partial x} = 0 \quad (8c)$$

$$-2C_2 \frac{\partial^2 v_1}{\partial t^2} - C_3 \frac{\partial^2 v_0}{\partial t^2} + \frac{M_{\theta z}}{R_m} - Q_{\theta z} + \frac{1}{R_m} \frac{\partial M_\theta}{\partial \theta} + \frac{\partial M_{x\theta}}{\partial x} = 0 \quad (8d)$$

$$-2C_1 \frac{\partial^2 w_0}{\partial t^2} + \frac{\partial Q_{xz}}{\partial x} - \frac{N_\theta}{R_m} + \frac{1}{R_m} \frac{\partial Q_{\theta z}}{\partial \theta} = 0 \quad (8e)$$

The extracted BCs are as the following:

$$\begin{aligned} \int \left(N_x d\theta + \frac{Q_{x\theta}}{R_m} dx \right) \delta u_0 &= 0; & \int \left(M_x d\theta + \frac{M_{x\theta}}{R_m} dx \right) \delta u_1 &= 0; & \int \left(Q_{x\theta} d\theta + \frac{N_\theta}{R_m} dx \right) \delta v_0 &= 0 \\ \int \left(M_{x\theta} d\theta + \frac{M_\theta}{R_m} dx \right) \delta v_1 &= 0; & \int \left(Q_{xz} d\theta + \frac{Q_{\theta z}}{R_m} dx \right) \delta w_0 &= 0 \end{aligned} \quad (9)$$

To perform the modal analysis the following BCs can be applied:

$$\text{Simple : } w_0 = 0, \quad v_0 = 0, \quad u_0 = 0, \quad M_x = 0, \quad M_{x\theta} = 0 \quad (10a)$$

$$\text{Clamped : } w_0 = 0, \quad u_0 = 0, \quad u_1 = 0, \quad v_0 = 0, \quad v_1 = 0 \quad (10b)$$

$$\text{Free : } N_x = 0, \quad M_x = 0, \quad Q_{x\theta} = 0, \quad M_{x\theta} = 0, \quad Q_{xz} = 0 \quad (10c)$$

By substituting Eqs. (1)-(4) into Eqs. (8), the equations of motion as a function of displacements are obtained as the following:

$$\begin{aligned} eq1 : & -2C_1 \frac{\partial^2 u_0}{\partial t^2} - C_3 \frac{\partial^2 u_1}{\partial t^2} + A_1 \frac{\partial^2 u_0}{\partial \theta^2} + A_2 \frac{\partial^2 u_0}{\partial x^2} + A_3 \frac{\partial^2 u_1}{\partial \theta^2} + A_4 \frac{\partial^2 u_1}{\partial x^2} + A_5 \frac{\partial^2 v_0}{\partial x \partial \theta} + A_6 \frac{\partial^2 v_1}{\partial x \partial \theta} \\ & + A_7 \frac{\partial w_0}{\partial x} = 0 \end{aligned} \quad (11a)$$

$$\begin{aligned} eq2 : & -2C_2 \frac{\partial^2 u_1}{\partial t^2} - C_3 \frac{\partial^2 u_0}{\partial t^2} + A_3 \frac{\partial^2 u_0}{\partial \theta^2} + A_4 \frac{\partial^2 u_0}{\partial x^2} + A_8 \frac{\partial^2 u_1}{\partial \theta^2} + A_9 \frac{\partial^2 u_1}{\partial x^2} + A_6 \frac{\partial^2 v_0}{\partial x \partial \theta} + A_{10} \frac{\partial^2 v_1}{\partial x \partial \theta} \\ & + A_{11} \frac{\partial w_0}{\partial x} + A_{12} u_1 = 0 \end{aligned} \quad (11b)$$

$$\begin{aligned} eq3 : & -2C_1 \frac{\partial^2 v_0}{\partial t^2} - C_3 \frac{\partial^2 v_1}{\partial t^2} + A_5 \frac{\partial^2 u_0}{\partial x \partial \theta} + A_6 \frac{\partial^2 u_1}{\partial x \partial \theta} + A_{13} \frac{\partial^2 v_0}{\partial \theta^2} + A_{14} \frac{\partial^2 v_0}{\partial x^2} + A_{15} \frac{\partial^2 v_1}{\partial \theta^2} + A_{16} \frac{\partial^2 v_1}{\partial x^2} \\ & + A_{17} \frac{\partial w_0}{\partial \theta} + A_{18} v_0 - R_m A_{18} v_1 = 0 \end{aligned} \quad (11c)$$

$$\begin{aligned} eq4 : & -2C_2 \frac{\partial^2 v_1}{\partial t^2} - C_3 \frac{\partial^2 v_0}{\partial t^2} + A_6 \frac{\partial^2 u_0}{\partial x \partial \theta} + A_{10} \frac{\partial^2 u_1}{\partial x \partial \theta} + A_{15} \frac{\partial^2 v_0}{\partial \theta^2} + A_{16} \frac{\partial^2 v_0}{\partial x^2} + A_{19} \frac{\partial^2 v_1}{\partial \theta^2} + A_{20} \frac{\partial^2 v_1}{\partial x^2} \\ & + A_{21} \frac{\partial w_0}{\partial \theta} - R_m A_{18} v_0 + R_m^2 A_{18} v_1 = 0 \end{aligned} \quad (11d)$$

$$eq5 : -2C_1 \frac{\partial^2 w_0}{\partial t^2} - A_{18} \frac{\partial^2 w_0}{\partial \theta^2} - A_{12} \frac{\partial^2 w_0}{\partial x^2} - A_7 \frac{\partial u_0}{\partial x} - A_{11} \frac{\partial u_1}{\partial x} - A_{17} \frac{\partial v_0}{\partial \theta} - A_{21} \frac{\partial v_1}{\partial \theta} - A_{13} w_0 = 0 \quad (11e)$$

where the coefficients A_1, \dots, A_{21} are reported in the [Appendix](#). Eqs. (11), contain a system of five linear coupled, homogeneous partial differential equations with constant coefficients.

3. Analytical solution

According to the equations and BCs, the response of Eqs. (11), can be considered as the following:

$$\begin{Bmatrix} u_0(x, \theta, t) \\ u_1(x, \theta, t) \\ v_0(x, \theta, t) \\ v_1(x, \theta, t) \\ w_0(x, \theta, t) \end{Bmatrix} = \begin{Bmatrix} a_1 \\ a_2 \\ a_3 \\ a_4 \\ a_5 \end{Bmatrix} \exp(\beta x + i\omega t) \begin{Bmatrix} \cos(n\alpha\theta) \\ \cos(n\alpha\theta) \\ \sin(n\alpha\theta) \\ \sin(n\alpha\theta) \\ \cos(n\alpha\theta) \end{Bmatrix}; \quad i = \sqrt{-1} \quad (12)$$

where ω and β are the natural frequency and eigenvalue, respectively and $\{a_1, a_2, a_3, a_4, a_5\}^T$ is the eigenvector. α is a coefficient that depends on the circumferential shape of the shell. When the cross-section of the shell is a full circle, $\alpha = 1$, and when it has a sector shape, it depends on the sector angle. By substituting [Eq. \(12\)](#), into the equations of motion ([Eq. 11](#)), a system of algebraic equations is obtained as the following:

$$\begin{bmatrix} m_{11} & m_{12} & m_{13} & m_{14} & m_{15} \\ m_{12} & m_{22} & m_{23} & m_{24} & m_{25} \\ -m_{13} & -m_{23} & m_{33} & m_{34} & m_{35} \\ -m_{14} & -m_{24} & m_{34} & m_{44} & m_{45} \\ -m_{15} & -m_{25} & m_{35} & m_{45} & m_{55} \end{bmatrix} \begin{Bmatrix} a_1 \\ a_2 \\ a_3 \\ a_4 \\ a_5 \end{Bmatrix} = \begin{Bmatrix} 0 \\ 0 \\ 0 \\ 0 \\ 0 \end{Bmatrix} \quad (13a)$$

$$\begin{aligned} m_{11} &= -A_1 \alpha^2 n^2 + A_2 \beta^2 + 2C_1 \omega^2; m_{12} = -A_3 \alpha^2 n^2 + A_4 \beta^2 + C_3 \omega^2; m_{13} = A_5 \beta \alpha n; m_{14} = A_6 \beta \alpha n \\ m_{15} &= A_7 \beta; m_{22} = -A_8 \alpha^2 n^2 + A_9 \beta^2 + 2C_2 \omega^2 + A_{12}; m_{23} = A_6 \beta \alpha n; m_{24} = A_{10} \beta \alpha n; m_{25} = A_{11} \beta \\ m_{33} &= -A_{13} \alpha^2 n^2 + A_{14} \beta^2 + 2C_1 \omega^2 + A_{18}; m_{34} = -A_{15} \alpha^2 n^2 + A_{16} \beta^2 + C_3 \omega^2 - A_{18} R_m; m_{35} = -A_{17} \alpha n \\ m_{44} &= -A_{19} \alpha^2 n^2 + A_{18} R_m^2 + A_{20} \beta^2 + 2C_2 \omega^2; m_{45} = -A_{21} \alpha n; m_{55} = -A_{18} \alpha^2 n^2 - A_{12} \beta^2 + 2C_1 \omega^2 - A_{13} \end{aligned} \quad (13b)$$

[Eq. \(13\)](#), is a system of homogeneous algebraic equations and for the nontrivial solution, the determinant of the coefficient matrix must be equated to zero which results in an algebraic equation of degree-ten with respect to β , and this equation is known as the dispersion equation. The dispersion equation contains ω as well. The roots of the dispersion equation are the eigenvalues and there is an eigenvector $\{V\}$, for each eigenvalue which they are functions of n , and ω . The general form of the solution is obtained as the following:

$$\begin{Bmatrix} u_0(x, \theta, t) \\ u_1(x, \theta, t) \\ v_0(x, \theta, t) \\ v_1(x, \theta, t) \\ w_0(x, \theta, t) \end{Bmatrix} = \begin{Bmatrix} \cos(n\alpha\theta) \\ \cos(n\alpha\theta) \\ \sin(n\alpha\theta) \\ \sin(n\alpha\theta) \\ \cos(n\alpha\theta) \end{Bmatrix} \exp(i\omega t) \sum_{j=1}^{10} d_j \{V\}_j \exp(\beta_j x) \quad (14)$$

where d_j are constant coefficients and they are determined from the BCs. By applying the BCs, ten algebraic equations are obtained as the following:

$$[M_{BC}]_{10 \times 10} \{d_1 \quad d_2 \quad \dots \quad d_{10}\}^T = \{0\}_{10 \times 1} \quad (15)$$

Table 1. Material and geometrical properties of composite shell.

Property (unit)	Quantity
Length (m)	$L = 1$
Middle radius (m)	$R_m = 0.16$
Inner layer thickness (mm)	$h_1 = 1$
Outer layer thickness (mm)	$h_3 = 1$
Core layer thickness (mm)	$h_2 = 5$
the length of the vertical cell rib to the length of the inclined cell rib ratio	$q/l = 2$
Inclined angle (degree)	$\varphi = 55$
The thickness of the cell wall to the length of the inclined cell rib ratio	$p/l = 0.0138571$
Young's modulus (GPa)	$E = 200$
Poisson's ratio	$\nu = 0.3$
Mass density (kg/m^3)	$\rho = 7800$

where the matrix of coefficient ($[M_{BC}]$) contains the natural frequency (ω). It should be mentioned that the matrix of coefficient contains the eigenvalues (the roots of the dispersion equation) as well, which can be substituted as a function of the natural frequency. For a nontrivial solution, the determinant of the matrix of coefficients ($[M_{BC}]$), equated to zero which results in a complicated algebraic equation. This equation is solved using the bisection method and the roots of this equation which are the natural frequencies are obtained.

4. Numerical solution

The natural frequencies of isotropic cylindrical shells are obtained using ANSYS FE software. For this purpose, the PLANE182 element in the axisymmetric model is employed which is an element with four nodes and two degrees of freedom at each node. The required mesh size is obtained using trial and error to vanish the sensitivity of the results to the mesh size variations.

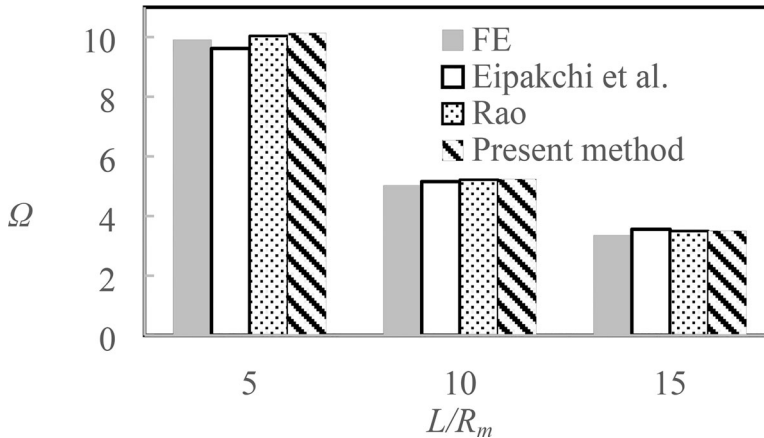
5. Results and discussion

To investigate the effects of different parameters such as the honeycomb structure characteristics and geometrical parameters on the frequency, a mathematical code has been provided in MAPLE software based on the presented analytical solution. The dimensionless natural frequency $\Omega = \omega(R_m^2/h)\sqrt{\rho/E}$ is defined where ω is the natural frequency (rad/s). The honeycomb structure parameters and geometrical properties of the auxetic composite shell have been reported in Table 1. All the reported results are based on the data in Table 1 except those are mentioned. The BCs are indicated with two letters in this text. C, S, and F stand for clamped, simply support, and free BCs, respectively. The first letter indicates the boundary condition at $x=0$, and the second letter determines the boundary condition at $x=L$.

To investigate the correctness of the presented method, Table 2 reports the dimensionless natural frequency of the isotropic cylindrical shell obtained by Viswanathan and Navaneethakrishnan (2003), Goncalves and Ramos (1997), Arnold and Warburton (1949), Smith and Haft (1968), Au-Yang (1978), and the presented method. Viswanathan and Navaneethakrishnan (2003) used the Love theory to obtain the natural frequency and Au-Yang (1978) used an approximation method based on the modal analysis and discretization to obtain the natural frequency. Goncalves and Ramos (1997) determined the natural frequency using the Budiansky-Sanders theory and FE method. Smith and Haft (1968) solved the equations of motion based on the Flugge theory analytically, and Arnold and Warburton (1949) obtained the natural frequency experimentally. It is observed that the present method has better results in comparison with the other references with respect to Arnold and Warburton (1949) which extracted the results experimentally. It should be

Table 2. Comparison of dimensionless natural frequency for isotropic cylindrical shells (C-C, $E = 183 \text{ GPa}$, $\rho = 7492 \text{ kg/m}^3$, $L = 0.5112 \text{ m}$, $R_m = 0.2162 \text{ m}$, $h = 1.5 \text{ mm}$).

n	Viswanathan and Navaneethakrishnan (2003)	Goncalves and Ramos (1997)	Arnold and Warburton (1949)	Smith and Haft (1968)	Au-Yang (1978)	Present method
2	51.461	55.660	49.124	56.611	58.830	48.936
3	88.740	87.987	85.174	92.503	93.652	86.260
4	153.394	158.623	157.276	164.090	164.288	155.010
5	248.076	251.959	250.374	257.505	257.664	253.982
6	361.498	366.489	365.657	372.392	372.234	364.631

**Figure 2.** Comparison of dimensionless axisymmetric natural frequency of isotropic cylindrical shells versus L/R_m (S-S, $E = 5.096 \text{ MPa}$, $R_m/h = 16$).

mentioned, to obtain the natural frequency for isotropic cylindrical shells, the thickness of the core layer (h_2) is zero.

Figure 2 compares the dimensionless axisymmetric natural frequency of isotropic cylindrical shells obtained by the FE method, Rao (2007), Eipakchi, Mahboubi Nasrekani, and Ahmadi (2020), and the present method. It is seen that the present method is in good agreement with the other references and FE method.

Figure 3 shows the variations of Poisson's ratio of the honeycomb structure versus φ for different values of q/l . It is seen that for negative values of φ and $q/l = 1, 2$ the Poisson ratios in both directions are negative and for positive values of φ and $q/l = 1, 2$ the Poisson ratios in both directions are positive. Of course, for $q/l = 0.5$ the behavior of the Poisson ratio does not follow a specific rule.

Table 3 compares the axisymmetric dimensionless natural frequency of auxetic composite cylindrical shells obtained by Eipakchi and Mahboubi Nasrekani (2020) and the present method. Eipakchi and Mahboubi Nasrekani (2020) used the CPT to extract the equations of motion and according to the CPT, the effect of shear deformations which is an important issue in the composite structures is not noticed.

Figure 4a shows the effect of R_m/h on the natural frequency of different auxetic composite shells with different thicknesses. In all cases, the thickness of the honeycomb core layer (h_2) is 60 percent of the total thickness (h). It is concluded that like the isotropic cylindrical

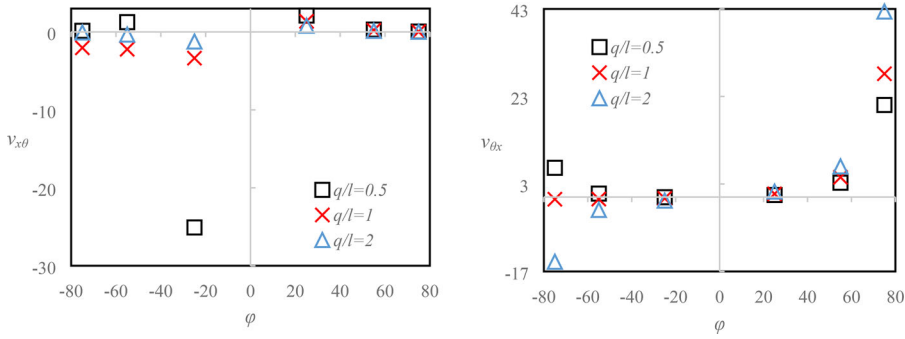


Figure 3. (a) Variations of $\nu_{x\theta}$ versus φ . (b) Variations of $\nu_{\theta x}$ versus φ .

shells, R_m/h does not have any remarkable effect on the natural frequency (Eipakchi, Mahboubi Nasrekani, and Ahmadi 2020). By substituting $n=0$, the results are obtained for the axisymmetric condition. Also, it can be concluded that the asymmetric frequency may be less than the axisymmetric natural frequency for some values of n . In other words, the axisymmetric frequency is not necessarily the minimum frequency. Besides, in the axisymmetric cases, the difference between the frequencies is less than the difference between the frequencies of asymmetric for the studied cases. Figure 4b shows the effect of R_m/h on the dimensionless natural frequency. Despite the Figure 4a results, it is seen that by increasing R_m/h , the dimensionless frequency increases.

Table 4 reports the effect of q/l on the dimensionless frequency and the mass of the core layer of the auxetic composite shell. It is observed that for positive values of φ , variations of φ and q/l do not have any significant effect on the dimensionless natural frequency and mass. The maximum frequency is for the case when $\varphi = 15$ and $q/l = 2$. The variations of the mass of the honeycomb layer in the interval of $\varphi < 0$ are more than the interval of $\varphi > 0$. The maximum effect of φ on the frequency and mass of the honeycomb layer is about 20% and 90%, respectively. Also, the maximum effect of q/l on the frequency and mass of the honeycomb layer is about 16% and 92%, respectively. Besides, by examining the frequency in terms of Poisson's ratio, it is observed that for the negative values of φ , by decreasing the Poisson's ratio, the frequency decreases, and for the positive values of φ , decreasing the Poisson ratio, increases the frequency.

Table 5 reports the effect of p/l on the dimensionless frequency and mass of the auxetic composite cylindrical shell. As a result, by increasing the thickness of the honeycomb cell wall, the mass of the honeycomb layer increases, and the frequency decreases. The maximum variations of frequency and mass due to the variations of p/l are 10% and 87%, respectively.

Table 6 shows the dimensionless frequency of auxetic composite shells under different boundary conditions. It is seen that the maximum frequency is attained for C-C boundary conditions. Note that for F-F and S-F boundary conditions, the first natural frequency is zero (rigid body motion/rotation) and only the bending frequencies are reported in Table 6.

Figure 5 shows the first two mode shapes of composite cylindrical shells for w_0 and u_0 . The boundary conditions for both edges are the same.

Figure 6 shows the first two mode shapes of composite cylindrical shells for w_0 and u_0 , for different boundary conditions at each edge as S-C, S-F, and C-F.

Table 7 reports the dimensionless first and second natural frequencies for auxetic composite cylindrical shells for different values of n . It is seen by increasing n , the natural frequency increases. Also, for the studied range, the asymmetric frequencies are less than their corresponding axisymmetric frequency.

Table 3. Comparison of dimensionless axisymmetric natural frequency of auxetic composite cylindrical shells (S-S).

h_1 (mm)	h_2 (mm)	h_3 (mm)	h (mm)	Dimensionless axisymmetric natural frequency	
				Eipakchi [33]	Present method
2	3	2	7	11.2341	11.6328
1.5	4	1.5	7	11.1095	11.5206
1	5	1	7	10.8696	11.3048
1.5	5	0.5	7	10.8648	11.3731
0.5	5	1.5	7	10.8630	10.9857

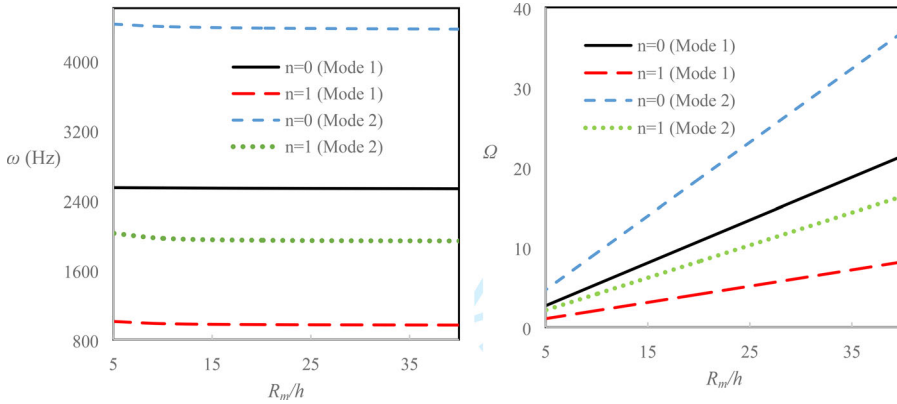


Figure 4. (a) Effect of R_m/h on natural frequency of auxetic composite shells (S-S). (b) Effect of R_m/h on dimensionless natural frequency of auxetic composite shells (S-S).

Table 4. Effects of q/l on dimensionless frequency and mass of auxetic composite shell (C-C, $n = 1$).

φ (Degree)	q/l	ν_{x0}	Ω	Mass of honeycomb layer (kg)
-55	0.5	1.25	-	-
	1	-2.22	3.714	7.857
	2	-0.34	4.327	1.597
-25	0.5	-25.08	3.644	9.677
	1	-3.36	4.345	1.557
	2	-1.23	4.440	0.757
-15	0.5	-14.90	4.210	2.907
	1	-4.84	4.399	1.137
	2	-2.06	4.456	0.637
15	0.5	4.73	4.425	0.917
	1	2.85	4.453	0.667
	2	1.59	4.473	0.497
25	0.5	2.10	4.435	0.807
	1	1.36	4.455	0.627
	2	0.80	4.472	0.487
55	0.5	0.30	4.416	0.897
	1	0.22	4.432	0.777
	2	0.14	4.447	0.667

Table 5. Effect of p/l on dimensionless natural frequency and mass of auxetic composite cylindrical shell (C-C, $n = 1$).

p/l	Ω	Mass of honeycomb layer (kg)
0.005	4.459	0.578
0.01	4.383	1.157
0.02	4.242	2.315
0.03	4.113	3.473
0.04	3.996	4.630

Table 6. Dimensionless frequency of auxetic composite cylindrical shell for different boundary conditions ($n = 1$).

S-F	C-F	F-F	C-C	S-S	S-C
4.4136	4.2481	4.4272	4.4349	4.2862	4.3067

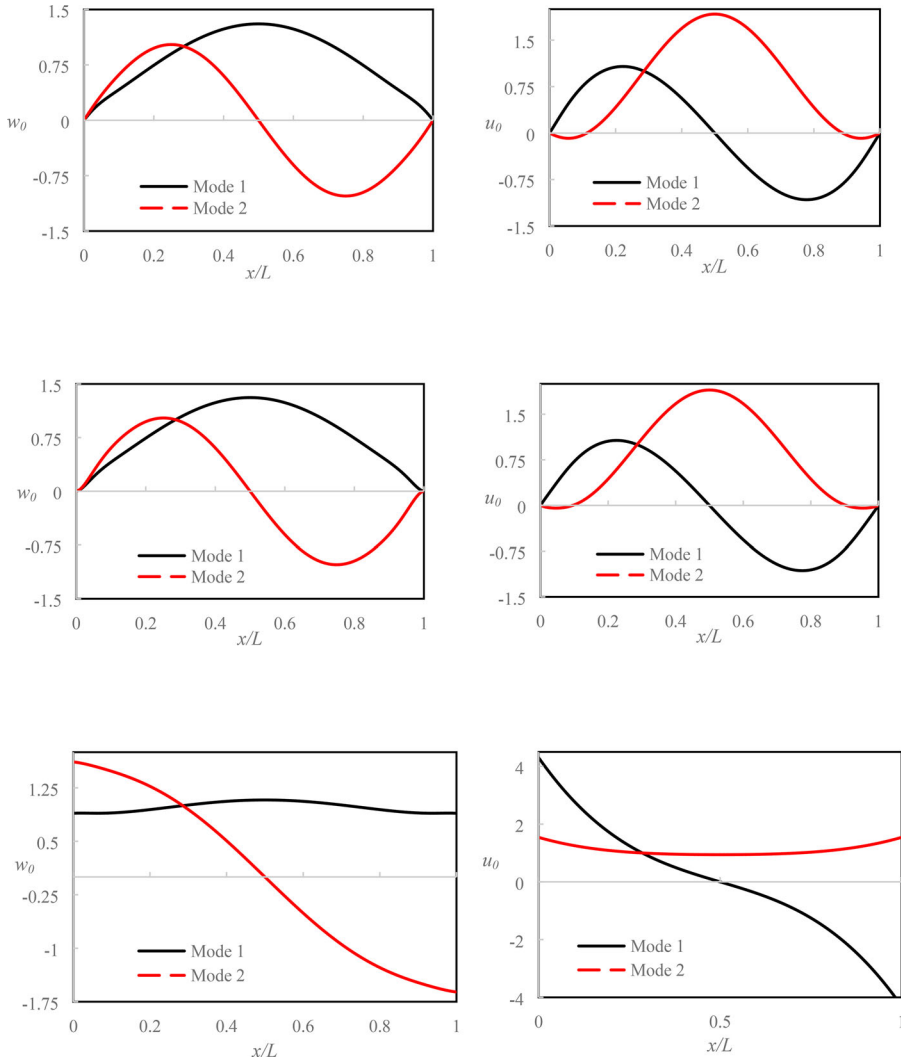


Figure 5. (a) Mode shape of S-S boundary conditions (w_0 , $n = 1$). (b) Mode shape of S-S boundary conditions (u_0 , $n = 1$). (c) Mode shape of C-C boundary conditions (w_0 , $n = 1$). (d) Mode shape of C-C boundary conditions (u_0 , $n = 1$). (e) Mode shape of F-F boundary conditions (w_0 , $n = 1$). (f) Mode shape of F-F boundary conditions (u_0 , $n = 1$).

To investigate the effect of the thickness of the honeycomb layer on the asymmetric natural frequency and the weight of the composite shell, Table 8 has been prepared. In all the cases the shells have the same volume. It is seen that by increasing the honeycomb core layer, the weight and the dimensionless asymmetric natural frequency of the auxetic composite shell decrease. In the studied cases, it can be concluded that by increasing the thickness of the core layer from case 1 (mm) to case 5 (mm), the weight decreases by about 64%, and the dimensionless asymmetric frequency decreases by about 3.5%, with respect to the case 1 (isotropic shell).

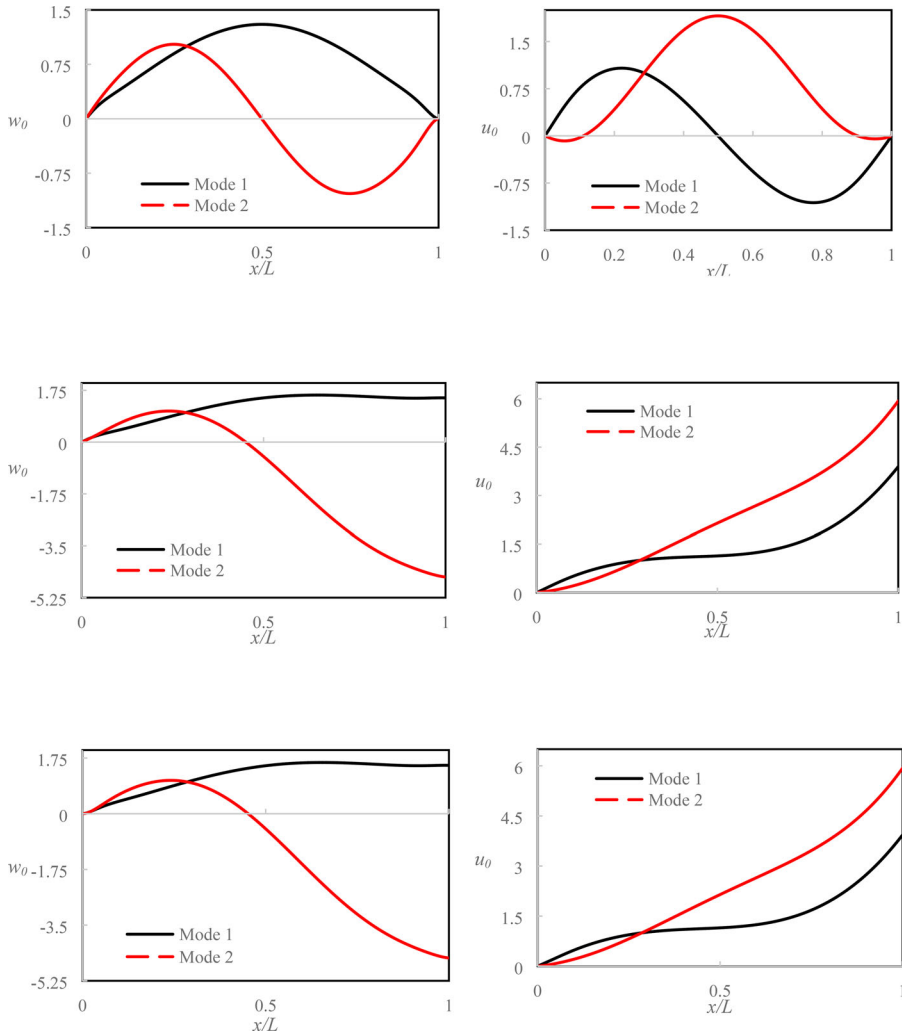


Figure 6. (a) Mode shape of S-C boundary conditions ($w_0, n = 1$). (b) Mode shape of S-C boundary conditions ($u_0, n = 1$). (c). Mode shape of S-F boundary conditions ($w_0, n = 1$). (d) Mode shape of S-F boundary conditions ($u_0, n = 1$). (e) Mode shape of C-F boundary conditions ($w_0, n = 1$). (f) Mode shape of C-F boundary conditions ($u_0, n = 1$).

Table 7. First and second dimensionless natural frequencies (C-C).

n	Mode 1	Mode 2
0	11.8250	20.5142
1	4.3272	8.6376
2	5.1366	11.2068
3	6.8077	11.4331
4	8.5834	16.2135
5	11.1187	23.0075

Table 8. Dimensionless asymmetric frequency for different auxetic composite and isotropic shells (C-C, $n = 1$).

	h_1 (mm)	h_2 (mm)	h_3 (mm)	h (mm)	Ω	Ratio of weight with respect to isotropic case
Case 1 (Isotropic)	3	0	3	6	5.2728	100%
Case 2 (Composite)	2.5	1	2.5	6	5.2547	84%
Case 3 (Composite)	2	2	2	6	5.2269	68%
Case 4 (Composite)	1.5	3	1.5	6	5.1799	52%
Case 5 (Composite)	1	4	1	6	5.0863	36%

6. Conclusion

An analytical method has been established to investigate asymmetric free vibrational behavior of auxetic composite cylindrical shells with honeycomb core layer. The governing equations were extracted based on the FSDT. Since the FE or experimental methods are time-consuming and complicated to analyze the honeycomb structures, this method can be useful and suitable to study these types of structures. By preparing the required inputs such as the material properties, geometry, and honeycomb parameters for the provided code, the results can be obtained readily. The effect of different geometrical and honeycomb structure parameters and different boundary conditions was studied using parametric analysis. Some of the conclusions can be listed as the following:

- For the negative values of inclined angle and $q/l = 1, 2$, the Poisson ratios are negative and for positive values of inclined angle and $q/l = 1, 2$, the Poisson ratios are positive and the maximum negative value for the Poisson ratio occurs when $q/l = 0.5$.
- R_m/h does not have any significant effect on the natural frequency of auxetic composite shells with honeycomb core layer while the dimensionless natural frequency increases as R_m/h increases.
- The axisymmetric frequency is not necessarily the minimum frequency and for some values of n , the asymmetric frequency is less than the axisymmetric natural frequency.
- By considering the asymmetric conditions, the difference between frequencies increases.
- When the inclined angle is negative, the weight of the honeycomb structure strongly depends on the honeycomb parameters (e.g. q/l , and φ).
- The maximum effects of φ and q/l on the frequency are 30% and 28%, respectively in the studied range.
- For the negative values of the inclined angle, by decreasing Poisson's ratio, the frequency decreases.
- For the positive values of the inclined angle, decreasing the Poisson ratio increases the frequency.
- The frequency of auxetic composite shell decreases as the thickness of the honeycomb cell wall increases.
- The maximum effect of honeycomb cell wall thickness on the frequency of auxetic composite shell is about 10%, in the studied range.
- For the studied cases, by increasing n , the natural frequency of asymmetric auxetic composite shell increases.
- As was expected, the maximum natural frequency occurs for C-C boundary conditions.
- From the viewpoint of the natural frequency, using the auxetic composite shells with the honeycomb core layer gives us this opportunity to use a light structure with almost the same characteristics. For the studied range of input data, by employing the auxetic composite shells the weight and asymmetric frequency decrease by about 64% and 3.5%, respectively with respect to the isotropic shells.

Disclosure statement

- The authors declare that they have no conflict of interest.
- All authors have materially participated in the research.
- This research received no specific grant from any funding agency in the public, commercial, or not-for-profit sectors.

ORCID

Hamidreza Eipakchi  <http://orcid.org/0000-0002-2405-0614>

Farid Mahboubi Nasrekani  <http://orcid.org/0000-0002-2970-439X>

References

- Akyuz, U., and A. Ertepinar. 1999. Stability and asymmetric vibrations of pressurized compressible hyperelastic cylindrical shells. *International Journal of Non-Linear Mechanics* 34 (3):391–404. doi:10.1016/S0020-7462(98)00015-8.
- Au-Yang, M. K. 1978. Natural frequency of cylindrical shells and panels in vacuum and in a fluid. *Journal of Sound and Vibration* 57 (3):341–55. doi:10.1016/0022-460X(78)90315-2.
- Bagheri, H., Y. Kiani, N. Bagheri, and M. R. Eslami. 2021. Free vibrations of functionally graded material cylindrical shell closed with two spherical caps. *Ships and Offshore Structures*:1–13. published online, doi:10.1080/17445302.2021.1889169.
- Bagheri, H., Y. Kiani, and M. R. Eslami. 2018. Free vibration of joined conical-cylindrical-conical shells. *Acta Mechanica* 229 (7):2751–64. doi:10.1007/s00707-018-2133-3.
- Banijamali, S. M., and A. A. Jafari. 2021. Free vibration analysis of rotating functionally graded conical shells reinforced by anisogrid lattice structure. *Mechanics Based Design of Structures and Machines*:1–23. doi:10.1080/15397734.2021.1881539.
- Biswal, D. K., and S. C. Mohanty. 2018. Free vibration and damping characteristics study of doubly curved sandwich shell panels with viscoelastic core and isotropic/laminated constraining layer. *European Journal of Mechanics – A/Solids* 72:424–39. doi:10.1016/j.euromechsol.2018.06.008.
- Chen, J. C., and C. D. Babcock. 1975. Nonlinear vibration of cylindrical shells. *AIAA Journal* 13 (7):868–76. doi:10.2514/3.60462.
- Eipakchi, H. R., and F. Mahboubi Nasrekani. 2020. Axisymmetric analysis of auxetic composite cylindrical shells with honeycomb core layer and variable thickness subjected to combined axial and non-uniform radial pressures. *Mechanics of Advanced Materials and Structures*:1–15. doi:10.1080/15376494.2020.1841346.
- Eipakchi, H. R., and F. Mahboubi Nasrekani. 2020. Response investigation of viscoelastic cylindrical shells with geometrical nonlinearity effect under moving pressure: An analytical approach. *Mechanics of Advanced Materials and Structures*:1–14. doi:10.1080/15376494.2020.1808916.
- Eipakchi, H. R., and F. Mahboubi Nasrekani. 2020. Vibrational behavior of composite cylindrical shells with auxetic honeycomb core layer subjected to a moving pressure. *Composite Structures* 254:112847. doi:10.1016/j.compstruct.2020.112847.
- Eipakchi, H. R., and F. Mahboubi Nasrekani. 2021. Geometrically nonlinear frequency analysis of composite cylinders with metamaterial honeycomb layer and adjustable Poisson's ratio using the multiple scale method. *Thin-Walled Structures* 169:108441. doi:10.1016/j.tws.2021.108441.
- Eipakchi, H. R., F. Mahboubi Nasrekani, and S. Ahmadi. 2020. An analytical approach for the vibration behavior of viscoelastic cylindrical shells under internal moving pressure. *Acta Mechanica* 231 (8):3405–18. doi:10.1007/s00707-020-02719-2.
- Ganapathi, M., and T. K. Varadan. 1996. Large amplitude vibrations of circular cylindrical shells. *Journal of Sound and Vibration* 192 (1):1–14. doi:10.1006/jsvi.1996.0172.
- Garg, A. K., R. K. Khare, and T. Kant. 2006. Higher-order closed-form solutions for free vibration of laminated composite and sandwich shells. *Journal of Sandwich Structures & Materials* 8 (3):205–35. doi:10.1177/1099636206062569.
- Gibson, L. J., and M. F. Ashby. 1997. *Cellular solids: Structure and properties*. 2nd ed. Cambridge, UK: Cambridge University Press.
- Goncalves, P. B., and N. R. S. S. Ramos. 1997. Numerical method for vibration analysis of cylindrical shells. *Journal of Engineering Mechanics* 123 (6):544–50. doi:10.1061/(ASCE)0733-9399(1997)123:6(544).
- Isvandzibaei, M. R., H. Jamaluddin, and R. I. Raja Hamzah. 2014. Frequency analysis of multiple layered cylindrical shells under lateral pressure with asymmetric boundary conditions. *Chinese Journal of Mechanical Engineering* 27 (1):23–31. doi:10.3901/CJME.2014.01.023.
- Javed, S., K. K. Viswanathan, and Z. A. Aziz. 2016. Free vibration analysis of composite cylindrical shells with non-uniform thickness walls. *Steel and Composite Structures* 20 (5):1087–102. doi:10.12989/scs.2016.20.5.1087.
- Khan, K., B. P. Patel, and Y. Nath. 2015. Free and forced vibration characteristics of bimodular composite laminated circular cylindrical shells. *Composite Structures* 126:386–97. doi:10.1016/j.compstruct.2015.02.022.
- Li, H., F. Pang, X. Miao, S. Gao, and F. Liu. 2019. A semi analytical method for free vibration analysis of composite laminated cylindrical and spherical shells with complex boundary conditions. *Thin-Walled Structures* 136: 200–20. doi:10.1016/j.tws.2018.12.009.
- Liu, Y. Z., Y. X. Hao, W. Zhang, J. Chen, and S. B. Li. 2015. Nonlinear dynamics of initially imperfect functionally graded circular cylindrical shell under complex loads. *Journal of Sound and Vibration* 348:294–328. doi:10.1016/j.jsv.2015.03.023.
- Liu, T., W. Zhang, J. J. Mao, and Y. Zheng. 2019. Nonlinear breathing vibrations of eccentric rotating composite laminated circular cylindrical shell subjected to temperature, rotating speed and external excitations. *Mechanical Systems and Signal Processing* 127:463–98. doi:10.1016/j.ymssp.2019.02.061.

- Liu, T., W. Zhang, and J. F. Wang. 2017. Nonlinear dynamics of composite laminated circular cylindrical shell clamped along a generatrix and with membranes at both ends. *Nonlinear Dynamics* 90 (2):1393–417. doi:10.1007/s11071-017-3734-4.
- Li, Y., W. Yao, and T. Wang. 2020. Free flexural vibration of thin-walled honeycomb sandwich cylindrical shells. *Thin-Walled Structures* 157:107032. doi:10.1016/j.tws.2020.107032.
- Li, R., X. Zheng, Y. Yang, M. Huang, and X. Huang. 2019. Hamiltonian system-based new analytic free vibration solutions of cylindrical shell panels. *Applied Mathematical Modelling* 76:900–17. doi:10.1016/j.apm.2019.07.020.
- Li, R., C. Zhou, and X. Zheng. 2021. On new analytic free vibration solutions of doubly curved shallow shells by the symplectic superposition method within the Hamiltonian-system framework. *Journal of Vibration and Acoustics* 143 (1):011002. doi:10.1115/1.4047701.
- Lopatin, A. V., and E. V. Morozov. 2019. Axisymmetric vibrations of the composite orthotropic cylindrical shell with rigid weightless end disks. *Thin-Walled Structures* 135:463–71. doi:10.1016/j.tws.2018.11.032.
- Mohammadimehr, M., and M. Mehrabi. 2017. Stability and free vibration analyses of double-bonded micro composite sandwich cylindrical shells conveying fluid flow. *Applied Mathematical Modelling* 47:685–709. doi:10.1016/j.apm.2017.03.054.
- Nekouei, M., M. Raghebi, and M. Mohammadi. 2019. Free vibration analysis of laminated composite conical shells reinforced with shape memory alloy fibers. *Acta Mechanica* 230 (12):4235–55. doi:10.1007/s00707-019-02501-z.
- Ozerciyes, V., and U. Yuceoglu. 2008. Free asymmetric vibrations of composite full circular cylindrical shells with a bonded central lap joint. *ASME International Mechanical Engineering Congress and Exposition*, Washington, DC; Paper No. IMECE2003-43661: 153–69. doi:10.1115/IMECE2003-43661.
- Raju, K. K., and G. V. Rao. 1976. Large amplitude asymmetric vibrations of some thin shells of revolution. *Journal of Sound and Vibration* 44 (3):327–33.
- Rao, S. S. 2007. *Vibration of continuous system*. New Jersey, USA: John Willey & Sons.
- Rn, A., and G. B. Warburton. 1949. Flexural vibrations of the walls of thin cylindrical shells having freely supported ends. *Proceeding of the Royal Society of London* 197:238–56.
- Sadd, M. H. 2009. *Elastic theory application and numeric*. UK: Elsevier Inc.
- Safarpour, M., A. R. Rahimi, and A. Alibeigloo. 2020. Static and free vibration analysis of graphene platelets reinforced composite truncated conical shell, cylindrical shell, and annular plate using theory of elasticity and DQM. *Mechanics Based Design of Structures and Machines* 48 (4):496–524. doi:10.1080/15397734.2019.1646137.
- Shahgholian-Ghahfarokhi, D., G. Rahimi, M. Zarei, and H. Salehipour. 2022. Free vibration analyses of composite sandwich cylindrical shells with grid cores: Experimental study and numerical simulation. *Mechanics Based Design of Structures and Machines* 50 (2):687–706. doi:10.1080/15397734.2020.1725565.
- Singh, B. N., D. Yadav, and N. G. R. Iyengar. 2002. Free vibration of composite cylindrical panels with random material properties. *Composite Structures* 58 (4):435–42. doi:10.1016/S0263-8223(02)00133-2.
- Sivadas, K. R., and N. Ganesan. 1991. Asymmetric vibration analysis of thick composite circular cylindrical shells with variable thickness. *Computers & Structures* 38 (5-6):627–35. doi:10.1016/0045-7949(91)90014-D.
- Smith, B. L., and E. E. Haft. 1968. Natural frequencies of clamped cylindrical shells. *Aiaa Journal* 6 (4):720–1. doi:10.2514/3.4570.
- Thinh, T. I., and M. C. Nguyen. 2016. Dynamic Stiffness Method for free vibration of composite cylindrical shells containing fluid. *Applied Mathematical Modelling* 40 (21-22):9286–301. doi:10.1016/j.apm.2016.06.015.
- Viswanathan, K. K., and P. V. Navaneethkrishnan. 2003. Free vibration study of layered cylindrical shells by collocation with splines. *Journal of Sound and Vibration* 260 (5):807–27. doi:10.1016/S0022-460X(02)00923-9.
- Wahl, L., S. Maas, D. Waldmann, A. Zurbes, and P. Freres. 2012. Shear stresses in honeycomb sandwich plates: Analytical solution, finite element method and experimental verification. *Journal of Sandwich Structures & Materials* 14 (4):449–68. doi:10.1177/1099636212444655.
- Wang, C., S. Cao, S. Lu, Z. Hu, L. Yao, and W. He. 2021. A CEL study of dynamic slamming response and failure mechanism on corrugated core composite-metal sandwich structures. *Ships and Offshore Structures*:1–24. doi:10.1080/17445302.2021.1906195.
- Wang, A., H. Chen, Y. Hao, and W. Zhang. 2018. Vibration and bending behavior of functionally graded nanocomposite doubly-curved shallow shells reinforced by graphene nanoplatelets. *Results in Physics* 9:550–9. doi:10.1016/j.rinp.2018.02.062.
- Wang, Z. W., B. Wu, Y. F. Wang, and S. M. Bosiakov. 2013. Analysis of fiberglass winding angle on natural frequency of free vibration of cylindrical shell with asymmetric boundary conditions. *Applied Mechanics and Materials* 274:65–9. doi:10.4028/www.scientific.net/AMM.274.65.
- Zhang, W., J. E. Chen, D. X. Cao, and L. H. Chen. 2014. Nonlinear dynamic responses of a truss core sandwich plate. *Composite Structures* 108:367–86. doi:10.1016/j.compstruct.2013.09.033.
- Zhang, W., Y. X. Hao, and J. Yang. 2012. Nonlinear dynamics of FGM circular cylindrical shell with clamped–clamped edges. *Composite Structures* 94 (3):1075–86. doi:10.1016/j.compstruct.2011.11.004.

Zhang, W., T. Liu, A. Xi, and Y. N. Wang. 2018. Resonant responses and chaotic dynamics of composite laminated circular cylindrical shell with membranes. *Journal of Sound and Vibration* 423:65–99. doi:10.1016/j.jsv.2018.02.049.

Zhang, W., S. W. Yang, and J. J. Mao. 2018. Nonlinear radial breathing vibrations of CFRP laminated cylindrical shell with non-normal boundary conditions subjected to axial pressure and radial line load at two ends. *Composite Structures* 190:52–78. doi:10.1016/j.compstruct.2018.01.091.

Zhu, X., J. Zhang, W. Zhang, and J. Chen. 2019. Vibration frequencies and energies of an auxetic honeycomb sandwich plate. *Mechanics of Advanced Materials and Structures* 26 (23):1951–7. doi:10.1080/15376494.2018.1455933.

Appendix

$$C_1 = \rho \left(\frac{h_1 + h_3}{2} + \frac{h_3^2 - h_1^2 + h_2(h_3 - h_1)}{4R_m} \right) + \frac{\rho^C h_2}{2}$$

$$C_2 = \rho \left(\frac{8(h_1^3 + h_3^3) + 12h_2(h_1^2 + h_3^2) + 6h_2^2(h_1 + h_3)}{48} + \frac{6(h_3^4 - h_1^4) + 12h_2(h_3^3 - h_1^3) + 9h_2^2(h_3^2 - h_1^2) + 3h_2^3(h_3 - h_1)}{48R_m} \right) + \frac{\rho^C h_2^3}{24}$$

$$C_3 = \rho \left(\frac{h_3^2 - h_1^2 + h_2(h_3 - h_1)}{2} + \frac{4(h_3^3 + h_1^3) + 6h_2(h_3^2 + h_1^2) + 3h_2^2(h_3 + h_1)}{12R_m} \right) + \frac{\rho^C h_2^3}{12R_m}$$

$$A_1 = \frac{G}{R_m} \left(\ln \left(\frac{2R_m + 2h_3 + h_2}{2R_m - 2h_1 - h_2} \right) + \ln \left(\frac{2R_m - h_2}{2R_m + h_2} \right) \right) + \frac{G_{x\theta}^C}{R_m} \ln \left(\frac{2R_m + h_2}{2R_m - h_2} \right)$$

$$A_2 = A(h_1 + h_3 + \frac{h_3^2 - h_1^2 + h_2(h_3 - h_1)}{2R_m}) + \frac{h_2 E_x^C}{1 - \nu_{x\theta}^C \nu_{\theta x}^C}$$

$$A_3 = G \left(\ln \left(\frac{2R_m - 2h_1 - h_2}{2R_m + 2h_3 + h_2} \right) + \ln \left(\frac{2R_m + h_2}{2R_m - h_2} \right) + \frac{h_1 + h_3}{R_m} \right) + G_{x\theta}^C \left(\ln \left(\frac{2R_m - h_2}{2R_m + h_2} \right) + \frac{h_2}{R_m} \right)$$

$$A_4 = A \left(\frac{h_3^2 - h_1^2 + h_2(h_3 - h_1)}{2} + \frac{4(h_3^3 + h_1^3) + 6h_2(h_3^2 + h_1^2) + 3h_2^2(h_3 + h_1)}{12R_m} \right) + \frac{E_x^C h_2^3}{12R_m(1 - \nu_{x\theta}^C \nu_{\theta x}^C)}$$

$$A_5 = \left(\frac{G}{R_m} + \frac{\lambda}{R_m} \right) (h_1 + h_3) + \frac{G_{x\theta}^C h_2}{R_m} + \frac{\nu_{x\theta}^C E_{\theta}^C h_2}{R_m(1 - \nu_{x\theta}^C \nu_{\theta x}^C)}$$

$$A_6 = \left(\frac{G}{2R_m} + \frac{\lambda}{2R_m} \right) (h_3^2 - h_1^2 + h_2(h_3 - h_1))$$

$$A_7 = \frac{\lambda}{R_m} (h_1 + h_3) + \frac{\nu_{x\theta}^C E_{\theta}^C h_2}{R_m(1 - \nu_{x\theta}^C \nu_{\theta x}^C)}$$

$$A_8 = G \left(R_m \ln \left(\frac{2R_m + 2h_3 + h_2}{2R_m - 2h_1 - h_2} \right) + R_m \ln \left(\frac{2R_m - h_2}{2R_m + h_2} \right) - (h_1 + h_3) + \frac{h_3^2 - h_1^2 + h_2(h_3 - h_1)}{2R_m} \right) + G_{x\theta}^C \left(R_m \ln \left(\frac{2R_m + h_2}{2R_m - h_2} \right) - h_2 \right)$$

$$A_9 = A \left(\frac{4(h_3^3 + h_1^3) + 6h_2(h_3^2 + h_1^2) + 3h_2^2(h_3 + h_1)}{12} + \frac{4(h_3^4 - h_1^4) + 8h_2(h_3^3 - h_1^3) + 6h_2^2(h_3^2 - h_1^2) + 2h_2^3(h_3 - h_1)}{16R_m} \right) + \frac{E_x^C h_2^3}{12(1 - \nu_{x\theta}^C \nu_{\theta x}^C)}$$

$$A_{10} = \left(\frac{G + \lambda}{12R_m} \right) \left[4(h_1^3 + h_3^3) + 6h_2(h_1^2 + h_3^2) + 3h_2^2(h_1 + h_3) \right] + \frac{G_{x\theta}^C h_2^3}{12R_m} + \frac{\nu_{x\theta}^C E_\theta^C h_2^3}{12R_m(1 - \nu_{x\theta}^C \nu_{\theta x}^C)}$$

$$A_{11} = \left(\frac{\kappa G}{2R_m} - \frac{\lambda}{2R_m} \right) (h_1^2 - h_3^2 + h_2(h_1 - h_3)) - \kappa G(h_1 + h_3) - \kappa G_{xz}^C h_2$$

$$A_{12} = \frac{\kappa G}{2R_m} (h_1^2 - h_3^2 + h_2(h_1 - h_3)) - \kappa G(h_1 + h_3) - \kappa G_{xz}^C h_2$$

$$A_{13} = \frac{A}{R_m} \left(\ln \left(\frac{2R_m + 2h_3 + h_2}{2R_m - 2h_1 - h_2} \right) + \ln \left(\frac{2R_m - h_2}{2R_m + h_2} \right) \right) + \frac{E_\theta^C}{R_m(1 - \nu_{x\theta}^C \nu_{\theta x}^C)} \ln \left(\frac{2R_m + h_2}{2R_m - h_2} \right)$$

$$A_{14} = G \left(h_1 + h_3 + \frac{h_3^2 - h_1^2 + h_2(h_3 - h_1)}{2R_m} \right) + G_{x\theta}^C h_2$$

$$A_{15} = A \left(\ln \left(\frac{2R_m - 2h_1 - h_2}{2R_m + 2h_3 + h_2} \right) + \ln \left(\frac{2R_m + h_2}{2R_m - h_2} \right) + \frac{h_1 + h_3}{R_m} \right) + \frac{E_\theta^C}{1 - \nu_{x\theta}^C \nu_{\theta x}^C} \left(\ln \left(\frac{2R_m - h_2}{2R_m + h_2} \right) + \frac{h_2}{R_m} \right)$$

$$A_{16} = G \left(\frac{h_3^2 - h_1^2 + h_2(h_3 - h_1)}{2} + \frac{4(h_3^3 + h_1^3) + 6h_2(h_3^2 + h_1^2) + 3h_2^2(h_3 + h_1)}{12R_m} \right) + \frac{G_{x\theta}^C h_2^3}{12R_m}$$

$$A_{17} = \left(\frac{A}{R_m} + \frac{\kappa G}{R_m} \right) \left(\ln \left(\frac{2R_m + 2h_3 + h_2}{2R_m - 2h_1 - h_2} \right) + \ln \left(\frac{2R_m - h_2}{2R_m + h_2} \right) \right) + \left(\frac{E_\theta^C}{R_m(1 - \nu_{x\theta}^C \nu_{\theta x}^C)} + \frac{\kappa G_{z\theta}^C}{R_m} \right) \ln \left(\frac{2R_m + h_2}{2R_m - h_2} \right)$$

$$A_{18} = \frac{\kappa G}{R_m} \left(\ln \left(\frac{2R_m - 2h_1 - h_2}{2R_m + 2h_3 + h_2} \right) + \ln \left(\frac{2R_m + h_2}{2R_m - h_2} \right) \right) + \frac{\kappa G_{z\theta}^C}{R_m} \ln \left(\frac{2R_m - h_2}{2R_m + h_2} \right)$$

$$A_{19} = A \left(R_m \ln \left(\frac{2R_m + 2h_3 + h_2}{2R_m - 2h_1 - h_2} \right) + R_m \ln \left(\frac{2R_m - h_2}{2R_m + h_2} \right) - (h_1 + h_3) + \frac{h_3^2 - h_1^2 + h_2(h_3 - h_1)}{2R_m} \right)$$

$$+ \frac{E_\theta^C}{1 - \nu_{x\theta}^C \nu_{\theta x}^C} \left(R_m \ln \left(\frac{2R_m + h_2}{2R_m - h_2} \right) - h_2 \right)$$

$$A_{20} = G \left(\frac{4(h_3^3 + h_1^3) + 6h_2(h_3^2 + h_1^2) + 3h_2^2(h_3 + h_1)}{12} + \frac{4(h_3^4 - h_1^4) + 8h_2(h_3^3 - h_1^3) + 6h_2^2(h_3^2 - h_1^2) + 2h_2^3(h_3 - h_1)}{16R_m} \right)$$

$$+ \frac{G_{x\theta}^C h_2^3}{12}$$

$$A_{21} = (A + \kappa G) \left(\ln \left(\frac{2R_m - 2h_1 - h_2}{2R_m + 2h_3 + h_2} \right) + \ln \left(\frac{2R_m + h_2}{2R_m - h_2} \right) \right) + \frac{A(h_1 + h_3)}{R_m} + \frac{E_\theta^C}{1 - \nu_{x\theta}^C \nu_{\theta x}^C} \left(\ln \left(\frac{2R_m - h_2}{2R_m + h_2} \right) + \frac{h_2}{R_m} \right)$$

$$+ \kappa G_{z\theta}^C \ln \left(\frac{2R_m - h_2}{2R_m + h_2} \right)$$